In Vivo Dynamic-Clamp Manipulation of Extrinsic and Intrinsic Conductances: Functional Roles of Shunting Inhibition and I_{BK} in Rat and Cat Cortex

Lyle J. Graham and Adrien Schramm

Abstract We present in vivo dynamic-clamp electrophysiological recordings to characterize the influences of shunting inhibition and the potassium current I_{BK} on the input–output (I/O) transfer function of cortical neurons, in response to both artificial (injected current or conductance) and functional visual stimuli. In comparison to previous experimental and theoretical studies, we find that realistic levels of shunting inhibition have a significant divisive effect on the firing gain. We also quantitatively characterize the effect of shunting inhibition on threshold and saturation. Shunting inhibition applied by dynamic-clamp also has a non-linear effect on visual responses, not only reducing the response but also significantly changing the timing of the response. We confirm predictions that I_{BK} facilitates spike firing, despite this being a hyperpolarizing current. This effect is demonstrated by an increase in both the gain of the I/O transfer function, e.g. the f/I curve, and visual responses.

1 Introduction

A myriad of biophysical mechanisms underly the dynamics of the single neuron, including those governed by intrinsic signals, such as voltage or the concentration of second messenger systems, and by extrinsic signals, notably neurotransmitters. These properties have been studied for decades with remarkable quantitative precision primarily in reduced in vitro preparations. As well illustrated in the chapters of this volume, dynamic-clamp protocols are proving to be valuable tools in the study of these mechanisms in vitro, alongside classical methods such as current- and voltage-clamp electrophysiology and pharmacological protocols.

L.J. Graham (✉)
Neurophysiology of Visual Computation Laboratory, Laboratory of Neurophysics and Physiology, CNRS UMR 8119, Université Paris Descartes, 45 rue des Saint-Pères, 75006 Paris, France
e-mail: lyle@biomedicale.univ-paris5.fr

A. Destexhe, T. Bal (eds.), *Dynamic-Clamp*, Springer Series in Computational Neuroscience 1, DOI 10.1007/978-0-387-89279-5_7,

Certainly a fundamental assumption of cellular neurobiology is that the complex dynamics measured in vitro are relevant for the qualitative and quantitative establishment of functional properties – thus how the neuron operates in its natural environment – with respect to its own particular processing and in the emergent behavior of the intact neural network. Nevertheless, firmly establishing the relationship between specific biophysical mechanisms and functional properties requires in vivo studies, and like the in vitro case dynamic-clamp promises to be a powerful method. This application is still new, with dynamic clamp only rarely used in in vivo protocols (Brizzi et al., 2004; Manuel et al., 2005 in cat spinal cord, Haider et al., 2007 in cat visual cortex) and, to our knowledge, never associated directly with the measurement of functional responses.

In this chapter we will present work in progress on applying dynamic-clamp methods in rat and cat cortex in vivo to study synaptic and cellular mechanisms participating in functional responses to visual input. Specifically, we examined the roles of two mechanisms, first, synaptic inhibition mediated by gamma-amino butyric acid ($GABA_A$) receptors, or "shunting" inhibition, and second, the calcium- and voltage-dependent potassium "BK" current that is implicated in shaping the spiking response of, mainly, excitatory cortical neurons. We studied how both mechanisms contribute to the basic input/output (I/O) characteristics of cortical neurons, and to the expression of visual receptive fields. While of course basic I/O characteristics are studied in the in vitro preparation, specifically the response to artificial electrophysiological inputs, the in vivo preparation allows the study of these properties under more physiological conditions, as well as making for a more direct link to the study of functional responses to sensory input, which in turn necessitates the intact preparation.

2 Shunting Inhibition and the Neuronal Response

The interaction between synaptic inhibition and excitation can be classified into two modes – subtractive (linear) or divisive (non-linear) – depending whether the inhibition can be approximated as a current source or a conductance change, respectively. In particular, since its reversal potential is relatively near the operating point of the neuron, the impact of inhibition mediated by $GABA_A$ receptors would be expected to result mainly by an increase in conductance, or shunt. Our work and others (visual cortex: Borg-Graham et al., 1998; Monier et al., 2003; Anderson et al., 2000; 2001; Hirsch et al., 1998; Marino et al., 2005; Priebe and Ferster, 2005, 2006; auditory cortex: Tan et al., 2004; Wehr and Zador, 2003, 2005; Zhang et al., 2003; barrel cortex: Higley and Contreras, 2006; Wilent and Contreras, 2004, 2005; prefrontal cortex: Haider et al., 2006) has shown that functionally evoked excitatory and inhibitory synaptic responses are often associated with significant conductance modulations driven by reversal potentials near that for $GABA_A$ inhibition. Often these

modulations are sufficiently strong, thus from one to three times the neuron's resting input conductance, to fundamentally change the time scales and integrative properties of the involved circuits, as predicted by modeling studies (Bernander et al., 1991; Rapp et al., 1992; Destexhe and Paré, 1999; Rudolph and Destexhe, 2003). Taken together, these results support the idea that strong $GABA_A$-mediated inhibition plays an important non-linear role in functional synaptic integration.

Many experimental and theoretical studies have directly explored the impact of shunting inhibition with respect to basic I/O function at the cellular level. These studies typically have been made in the context of "background" synaptic activity, including those that employed dynamic-clamp-simulated synaptic input in vitro (Chance et al., 2002; Kreiner and Jaeger, 2003; Mitchell and Silver, 2003). These works have resulted in diverse interpretations: While some have presented evidence that $GABA_A$ inhibition affects I/O gain (Ingham and McAlpine, 2005), others have shown that at the spiking level the effect of shunting inhibition is mainly subtractive, thus linear, with respect to how many spikes are produced by a given level of excitatory input (Holt and Koch, 1997; Ulrich, 2003; Brizzi et al., 2004). Other studies have shown an explicit divisive effect of shunting inhibition, but only when the synaptic input is fluctuating, or "noisy" (Chance et al., 2002; Mitchell and Silver, 2003), or when dendritic non-linear integration is considered (Capaday and Van Vreeswijk, 2006), or with both conditions, thus fluctuating input in dendrites (Prescott and De Koninck, 2003).

To clarify these questions, we investigated the quantitative role of shunting inhibition in vivo on the I/O transfer function and on visual responses in rat and cat visual cortex, using the dynamic-clamp protocol. In particular, we wanted to establish the essential nature of the interaction between shunting inhibition and excitation, without making assumptions on the input dynamics. Our results confirmed that simulated shunting inhibition, at strengths consistent with that evoked during visual responses and with no a priori temporal structure (e.g. step inputs), has a significant non-linear as well as linear effect on the basic I/O transfer function of cortical neurons.

A large body of work has focused on the important question of how dynamical variability in the neuron state, broadly defined as "noise," affects I/O properties. For example, earlier studies have demonstrated the qualitative impact of membrane voltage fluctuations per se on the I/O relation of neurons, which may arise from distinct interactions with, on one hand, the conductance state of the cell and, on the other, the threshold characteristics of the spike mechanism (Fellous et al., 2003). In our experiments, we explicitly wanted to minimize the role of fluctuations in the effect of shunting inhibition. Not only does the use of simple inputs help establish a baseline for the effect of shunting inhibition, under some conditions tonic activation of $GABA_A$ receptors may have an important functional consequence (Stell et al., 2003; Semyanov et al., 2004). Our preliminary results also indicate that artificial shunting inhibition applied during the visual response has an effect that is more

complex than a simple reduction of spike output, and thus can modulate the timing of the response.

3 The BK Current and the Neuronal Response

The pattern of spike responses following a given input are determined in large part by the complex interaction of a neuron's intrinsic membrane channels. In particular, diverse potassium channels in a given cell type may span a large range of kinetic timescales, allowing the identification of specific dynamical characteristics of the spike output with specific channel types. As an example, the timing of spikes emitted by regular adapting, typically excitatory, neurons (following the physiological classification of neurons according to their firing patterns in response to sustained current inputs, e.g. McCormick et al., 1985) is characterized by three different time scales of adaptation of their firing frequency, roughly tens of milliseconds, hundreds of milliseconds, and one or more seconds. Furthermore, each time scale is associated primarily (but not exclusively) with specific K^+ currents with complementary kinetics, respectively the BK current (I_{BK}), the M current, and the after-hyperpolarization (AHP) current (reviewed in Storm, 1990). The M and AHP currents are increasingly activated with each additional spike, so that these hyperpolarizing K^+ currents act in the standard fashion to progressively counteract the depolarizing stimulation current.

The role of I_{BK}, in contrast, appears to be opposite to this classical action of K^+ current on spike firing. The large conductance BK channels (also called BKCa, KCa1.1, MaxiK, *Slo*) (Vergara et al., 1998) underlying I_{BK}, whose activation and inactivation are Ca^{2+} and voltage dependent, are found in different neuronal types including regular adapting cortical and hippocampal pyramidal cells. Various earlier studies have suggested that a downregulation of I_{BK}, either from experimental pharmacological manipulations or secondary to pathological conditions, is associated with increased excitability (reviewed in Gu et al., 2007). From our own theoretical modeling, we have proposed an explicit connection between this current and excitability, thus that fast firing adaptation in regular adapting neurons – the initial slowing of firing frequency over the first ten or so spikes – is due to the *removal*, not enhancement, of I_{BK} (Graham, 2006, 2007). First, we propose that the shortening of the spike by activation of I_{BK} during spike repolarization reduces the activation of other, slower, K^+ currents. Second, modeling (Borg-Graham, 1987, 1999) has predicted that at the end of spike repolarization I_{BK} inactivates extremely quickly, giving rise to the fast after-hyperpolarization (fAHP) in this cell type. This inactivation is much faster than that of other K + currents, thus when there is a prevalence of I_{BK} this allows a more rapid subsequent depolarization to continued stimulation, and thus more rapid firing of the next spike. Third, the local hyperpolarization caused by somatic I_{BK} is

immediately counteracted by dendritic charge, accounting in part for the depolarizing phase of the fAHP. In the case of a constant depolarizing current, this results in a faster charging of the soma membrane as compared to the response to the stimulus current alone (Borg-Graham, 1987, 1999; Storm et al., 1987). Fourth, the relatively hyperpolarized peak of the fAHP due to I_{BK} contributes to the removal of inactivation of the transient Na^+ current underlying the spike, and thus lowering spike threshold for the next spike. Finally, to account for the disappearance of the fAHP after several spikes, our model predicted that I_{BK} de-activates after several spikes, subsequently allowing other, slower, K^+ currents to dominate and to reduce the firing frequency (Borg-Graham, 1987, 1999). These ideas were supported by our earlier work measuring how I_{BK} modulates spike shape (Shao et al., 1999; specifically Figs. 3 and 6) in hippocampal pyramidal cells. This hypothesis was more explicitly explored in recent work by Storm and colleagues (Gu et al., 2007), who showed that pharmacological blocking of I_{BK} during in vitro recordings in hippocampal pyramidal cells strongly reduces the frequency of the first few spikes in a spike train evoked by a constant current step.

The experimental results to date, however, cannot establish a direct link between I_{BK} and spike frequency, simply because pharmacological manipulations may impact multiple mechanisms. We have therefore studied these predictions at the biophysical level, by combining pharmacological methods with dynamic-clamp, in order to show that I_{BK} alone can account for an acceleration of neuronal firing. Thus, we recorded from regular adapting cortical neurons with pipettes containing the fast Ca^{2+} buffer BAPTA. BAPTA prevents a sufficient increase of the intracellular Ca^{2+} concentration during a spike to activate I_{BK}, thus effectively reducing or even disabling this current (Velumian and Carlen, 1999). In our protocol we verified the control firing properties of the recorded cell immediately after whole-cell access before diffusion of BAPTA. We then continued to make f/I sequences to see if the expected disappearance of the fAHP, as an indication of a blocked I_{BK}, is correlated with a reduction of both fast adaptation and the peak firing rate. The next step was to restore a phenomenological I_{BK} by using a dynamic-clamp model inspired from that proposed from our earlier work (Borg-Graham, 1987, 1999; Shao, et al., 1999). In this manner, the fast adapting component of the recorded cell may be added or removed at will during subsequent protocols. We then explored how fast adaptation influences visual processing by comparing the spike response to a given visual stimulation with and without the dynamic-clamp I_{BK} model. Specifically, we propose that I_{BK} acts to both increase and to phase advance the response for stimulus durations – tens to one hundred milliseconds – that correspond to natural vision. Thus I_{BK}, and by extension pathways that modulate it in vivo, may dynamically adjust the response of excitatory neurons, perhaps qualitatively changing the receptive field type when considered with the dynamics of synaptic input tuning over the same timescales.

4 Methods

4.1 Animal Preparations

All experimental protocols described here were made in order to maximize the animal's well-being and comfort, and have been approved by the Direction Départementale des Services Vétérinaires. Sprague–Dawley Rats (male, 300–500 g) were anesthetized with urethane (1.5 g/kg i.p.). Young adult male cats (3.2–4.2 kg) were initially anesthetized with an injection of ketamine and xylazine (1 and 10 mg/kg, respectively, i.m.). Cats were intubated for artificial respiration and fitted with a urinary catheter. All surgical manipulations (incisions, pressure points) were preceded by local injections of lidocaine. After surgical preparation and anesthesia induction, animals were placed in a stereotaxic holder (Narishige model SN-3 N). In the case of cats, anesthesia was maintained by intravenous perfusion of propofol (5 mg/kg/h for anesthesia) and sufentanil (0.004 mg/kg/h for analgesia), delivered in Ringer 5% glucose. Rate and volume of the respiration pump was adjusted as necessary to maintain a relative PCO_2 between 3 and 4.5%. In order to eliminate natural eye movements, cats were paralyzed by an induction dose of pancuronium (0.3 mg/kg), followed by a continuous perfusion of pancuronium (0.3 mg/kg/h) delivered in Ringer 5% glucose solution. For cats, in order to reduce respiratory movement at the cortex, a bilateral pneumothorax was performed. For cats, gas-permeable contact lenses (Metro Optics) were used to prevent cornea degradation, with local application of atropine methyl nitrate (for pupil dilation) and neosenephrine (to retract the nictitating membrane), and correction lenses were chosen as appropriate to focus back-projections of the optic disc on the visual stimulus display. Rectal temperature was monitored and maintained in both rat and cat at 37.5 $\pm$ 0.5°C by a heating blanket (CWE Instruments). Heart rate was monitored to indicate the depth of the anesthesia, and as necessary supplemental urethane was injected i.p. (rat) or adjustment of propofol perfusion (cat). For whole-cell patch recordings, craniotomies were performed either above the somatosensory cortex (rat) or above the primary visual cortex (both animals). Experiments typically lasted for 5–6 h for rats and 2–3 days for cats. At the end of each experiment euthanasia was performed with an overdose injection of sodium pentobarbital (i.p. rat or i.v. cat).

4.2 Computational Implementation

Experiment control software (Surf Lab, in-house software) including visual response data acquisition and dynamic-clamp protocols was made with the LabVIEW system (v7.1, National Instruments). The dynamic-clamp software was based on the G-clamp system (v1.2, Kullmann et al., 2004), also written in LabVIEW. Data acquisition was made at 40 khz for both current and voltage, and update of the dynamic-clamp current command was also nominally at 40 khz.

The entire system (Fig. 1) consisted of three computers, including an "executive" computer running Windows XP (Dell Precision 650 – Intel Xeon 2.66 Ghz, 1.5 GB RAM) which ran the Surf Lab and G-clamp programs simultaneously, a real-time computer (generic computer based on an Intel Pentium 4 3.2 Ghz processor with 1 GB RAM) implementing the actual dynamic-clamp routines, and a second Windows XP computer dedicated to generating visual stimuli (Dell Optilex GX620 – Intel Pentium 4 3,2 Ghz, 1 GB RAM). Communication between the executive computer and the dynamic-clamp computer (commands from executive to dynamic-clamp; data from dynamic-clamp to executive), and between the executive and the visual computers (commands from the executive to the visual) was made by a TCP/IP serial link. Synchronization timing from the visual computer for the executive computer was made via a dedicated line

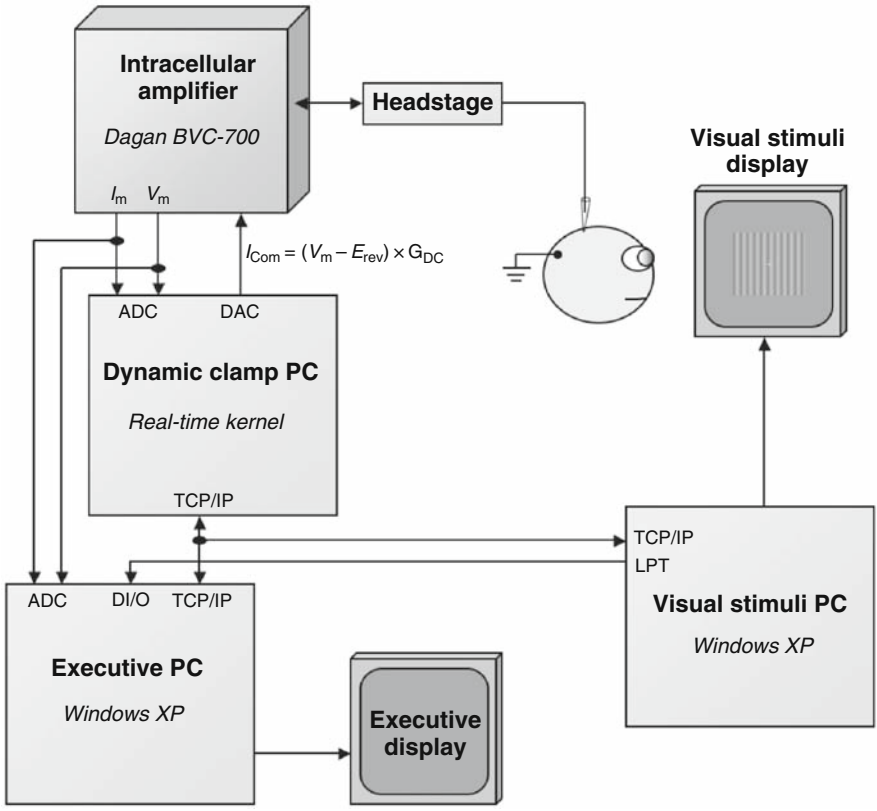

Fig. 1 System diagram of the in vivo dynamic-clamp system. ADC – analog–digital converter, DAC – digital analog converter, DI/O – digital input/output port, TCP/IP – TCP/IP serial port, LPT – parallel (line printer) port, I_m – membrane current amplifier output, V_m – membrane voltage amplifier output, I_{Com} – membrane current command amplifier input, G_{DC} – dynamic-clamp conductance model, E_{rev} – reversal potential of G_{DC}

from the parallel port (LPT) on the visual computer, and read on a digital I/O line on the data acquisition card of the executive computer.

The Surf Lab LabVIEW program controlled the visual experiments, and the G-clamp LabVIEW program controlled the dynamic-clamp routines. G-clamp has two components, one that includes the user and file system interface that runs on the executive computer, and one which runs on the real-time computer (under a real-time kernel, Pharlap), with a real-time version of LabVIEW. Surf Lab was used alone for running visual protocols under either current or voltage clamp. G-clamp was used alone for running current-clamp and dynamic-clamp protocols aimed primarily at measuring intrinsic properties, such as *f–I* and *f–G* curves. Finally, G-clamp was modified to include a continuous running mode, which allowed a particular dynamic-clamp conductance to be applied in the background while a visual protocol was simultaneously run under the control of Surf Lab.

Visual stimulation was generated using the VisionEgg software package (Straw et al., 2006). For a given protocol, stimulation parameters were sent to the visual stimulus computer from the executive computer running Surf Lab, followed by stimulus timing information sent in the opposite direction over the LPT line. Stimulus patterns typically consisted of moving sinusoidal gratings with a temporal frequency between 1 and 4 Hz, a spatial frequency typically between 0.1 and 0.8 cycles per degree, masked with a Gaussian window with width (sigma) between 10 and 40°. Orientation dependence was measured with gratings whose directions varied over 360° at increments of 45°, presented in random order for durations ranging from 0.5 to 2 s. The results presented here are from gratings with a contrast of 100%.

Whole-cell patch recordings were made with a Dagan Instruments BVC-700 intracellular amplifier. The membrane voltage output was low-pass filtered at 10 kHz with the amplifier's built-in filter, and the dynamic-clamp-calculated current was controlled via the amplifier's current command input in current-clamp mode.

4.3 Dynamic-Clamp Models for Shunting Inhibition and $\mathbf{I}_{BK}$

Our present study of how shunting inhibition affects firing properties uses the simplest possible model for the synapse, namely an imposed conductance with a reversal potential of –70 mV, applied either as a constant conductance step in the case of measuring firing rate in response to simultaneous excitatory conductance steps (reversal potential 0 mV), or as a continuous conductance during the measurement of visual responses.

Our study of I_{BK} employs dynamic-clamp to provide an intermediate channel model, specifically one that is not a conductance model in the standard sense. The native I_{BK} channel is co-localized with calcium channels (predicted by Borg-Graham, 1987, 1991, and subsequently verified by Marrion and Tavalin,

1998), allowing for a fast and sensitive dependence on calcium entry during the spike. In the I_{BK} model used here, this dependence on nearby calcium entry was implicit by turning on the current at the beginning of spike repolarization, defined solely in terms of the voltage trajectory. Once turned on, the I_{BK} model provided a fixed, predefined repolarizing current, typically on the order of 2–4 nA. The I_{BK} model was then turned off when the membrane voltage reached a fixed, predefined value, typically –60 mV, equivalent to the minimum value of the fAHP. As a final simplification, in the results presented here, there is no inactivation of the I_{BK} model, contrary to the real I_{BK}. Despite these simplifications, as shown in Fig. 5, the amplitude and duration of this basic model is consistent with the dynamics predicted by a biophysically detailed model.

An important motivation of this approach is that the resulting dynamic-clamp current is less susceptible to inevitable electrode artifacts. Thus, given the large current and fast dynamics of the biophysical model prediction, a true conductance model will be much more prone to "ringing" at onset and de-activation than the simple model. Future work will address these challenges to allow a more sophisticated and accurate I_{BK} dynamic-clamp model, e.g. by incorporating a predictive model of the electrode artifact (e.g. with the methods described in the chapter by Brette et al.) in the I_{BK} model to distinguish online the expected "true" membrane voltage from the signal arising from the incompletely compensated electrode circuit.

4.4 Electrophysiological Recordings

All recordings were done with the blind whole-cell patch-clamp technique in vivo, following protocols described previously (Borg-Graham, et al., 1998). We used both thick wall borosilicate glass capillaries with filaments and thin wall borosilicate glass capillaries without filaments to make the pipettes (respectively OD 1.5 mm, ID 0.84 mm and OD 1.5 mm, ID 1.12 mm, World Precision Instruments). Pipettes were pulled in a horizontal puller (Sutter Instruments model P-97) in three steps in order to have a small tip ($\sim$2 μm) and a long and thin taper. Pipette resistance prior to recording was kept to between 5 and 8 MΩ. Pipettes were filled with a solution containing (in mM) K-gluconate 140, KCl 4, Hepes 10, $MgCl_2$ 2, ATP 4, GTP 0.4, EGTA 0.5 and, depending on the case, 0.01% DMSO and 10 mM BAPTA. The osmolarity of the intracellular solution was adjusted to 285–295 mOsmol, and the pH was set to 7.2–7.5.

Whole-cell patch electrodes were introduced into the cortex under current-clamp mode, using a –1 nA amplitude, 10 Hz 50% duty cycle current pulse train to monitor the change in resistance as the electrode approached a cell, and with the amplifier bridge circuit balanced to compensate for the electrode resistance. For penetration of the cortical surface, the electrode was initially advanced using a motorized micromanipulator (Narishige model SM-21) in continuous

mode (~250 μm/s), with a positive pressure of 100–300 mmHg applied to the interior of the pipette. After penetration of the cortical surface was detected by a transient deflection of the measured voltage, the electrode was advanced until a predetermined depth (100–2,000 μm) was reached. The electrode was then retracted in continuous mode for 100–200 μm, and the positive pressure immediately reduced to 40–70 mmHg. The voltage offset was then adjusted according to the tip offset potential (–14 mV measured with our K-gluconate solution). The electrode was then advanced in 3–4 μm steps until a deflection of the voltage response equivalent to 5–10% of the unbalanced response was observed, reflecting contact with a cell membrane. At this point the positive pressure was removed and whole-cell access achieved by one of two methods. The first method maintained the 1 nA current pulse train, resulting in spontaneous electroporation of the membrane within several seconds as a result of large voltage fluctuations following giga-seal formation (Schramm and Graham, 2007). The second, more traditional, method was made by monitoring slow formation of the giga-seal with small (100 pA) current pulses, followed by brief application of suction on the pipette interior.

4.5 Bridge Balance – Estimation of Access Resistance

A fundamental challenge for single patch electrode dynamic-clamp protocols is the accurate online estimation and correction of the access resistance once in the whole-cell patch configuration. The first step for achieving this was to adjust the capacitance compensation on the amplifier during applied current pulses in current-clamp mode to the maximum degree without inducing oscillations. In our protocols we then used two criteria in current-clamp mode for the subsequent estimation of the bridge component (Borg-Graham et al., 1998): First, reasonable estimates of the bridge component are possible when there is a clear distinction of the electrode versus cell time constants during the response to a subthreshold hyperpolarizing or depolarizing current step (typically ±100 pA). Once the bridge is adjusted according to the differential time constants, the estimate was verified by noting any change in the height of the initial spike in response to a series of increasing suprathreshold current steps. Thus, a good estimate of the access resistance and subsequent stability of the compensation was contingent on a variation of spike height less than approximately 5 mV over a several hundred picoampere range of current step amplitudes. In our experience, adequate estimation and subsequent cancelation with the bridge balance adjustment of the amplifier necessitates an access resistance below 40–50 MΩ.

A typical example of the distinct bridge (electrode) and cell components that we find in the response to a current step is shown in Fig. 5, in the context of the I_{BK} dynamic-clamp protocols. In the center panels the voltage response (upper panel) is shown to a depolarizing 500 pA current pulse (lower panel), from a whole-cell patch recording made in rat somatosensory cortex in vivo. In this

trace the I_{BK} dynamic-clamp model is turned on, as indicated by the 4 nA hyperpolarizing pulse during the repolarizing phase of the action potential. In this example, the access resistance was estimated to be 26 MΩ, with a resting input resistance of the neuron of 55 MΩ. A small fast bridge component is seen at the start of the depolarizing current pulse, followed by larger but still very fast bridge components on the leading and trailing edges of the large model I_{BK} pulse. The much slower response component of the neuron's "linear" response – the linear membrane time constant of this cell was estimated at 9.5 ms – can be appreciated by the trajectory of the depolarizing voltage response over many milliseconds prior to the action potential.

5 Results

5.1 The Effects of Shunting Inhibition on the Input–Output Function and Visual Responses

To evaluate the quantitative effect of shunting inhibition on the I/O relation of a neuron, we applied conductance steps comprised of different combinations of artificial excitatory and inhibitory components, while measuring the resulting spike trains. Excitatory steps (reversal potential = 0 mV) and inhibitory steps (reversal potential = –70 mV) were calibrated relative to each neuron's resting input conductance, thus Gex(rel) and Ginh(rel). This procedure facilitated comparisons of firing properties across diverse cell populations, notably over a range of resting input resistances. Intrinsic noise was estimated by measuring the standard deviation of the membrane voltage at rest. Quantitative fits to *f–G* characteristics were made with a sigmoid expression, after excluding responses past firing saturation, if any, with gain defined as the maximum slope of the sigmoid fit. Saturation was estimated directly from the asymptotic maximum of the fitted sigmoid, whenever the fit showed a significant deceleration after the maximum slope.

Figure 2 shows *f–G* characteristics for increasing steps of constant dynamic-clamp excitatory "synaptic" conductance, with different levels of simultaneous shunting "synaptic" conductance. Increasing levels of shunting inhibition, Ginh(rel), tended to shift the *f–G* curve to the right – thus a linear interaction with the excitatory input – as well as reduce the slope or gain of the characteristic – thus a non-linear interaction with the excitatory input. This figure also shows two example traces, with excitation alone (bottom left) and with added shunting inhibition (bottom right), in the latter case with the excitation sufficient to give approximately the same number of spikes as the no inhibition condition. These traces show explicitly how shunting inhibition significantly diminishes the efficacy of a depolarizing current: In part because of the strongly amplified negative currents during each spike supplied by the inhibition, the average level of depolarizing current for evoking the same number of spike is significantly larger than when there is no inhibition.

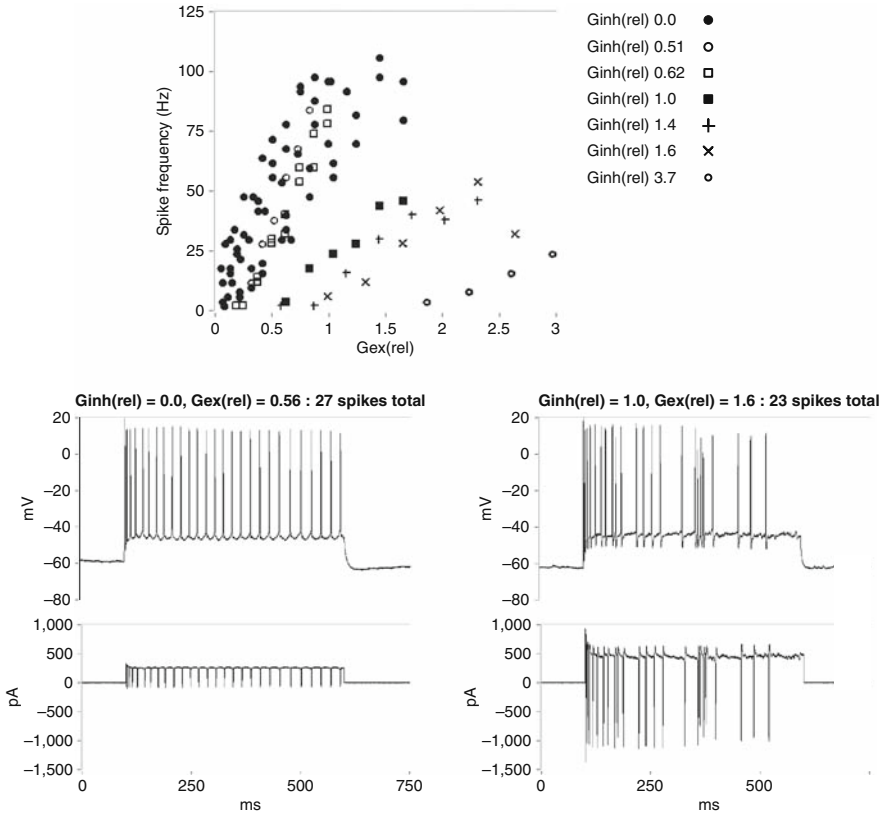

Fig. 2 The effect of dynamic-clamp "shunting inhibition" on the *f–G* characteristic of a regular adapting neuron recorded in rat cortex in vivo. *Top*: *f–G* characteristics measured with simultaneous steps of shunting inhibition ranging from 0 to 3.7 (values normalized to the neuron's resting conductance). *Bottom left*: Voltage and dynamic-clamp current in response to a pure excitatory "synaptic" conductance step, Gex(rel) = 0.56. *Bottom right*: Voltage and dynamic-clamp current in response to a conductance step combining an excitatory "synaptic", with Gex(rel) = 1.6, and shunting "synaptic" conductance with Ginh(rel) = 1.0, giving approximately the same number of evoked spikes as Gex(rel) = 0.56 with no inhibition

Figure 3 shows population results from a total of 27 regular adapting neurons recorded in vivo in rat and cat cortex, quantifying the effect of shunting inhibition on firing properties measured with *f–G* protocols. The dependence of *f–G* gain on inhibition (top left) and the dependence of Gex(rel) threshold on inhibition (top right) summarize the most basic non-linear and linear interactions, respectively, between excitation and inhibition, at least with respect to average firing over 500 ms of constant input. Quantitatively, the non-linear effect over the population is given by an average normalized sensitivity of –0.44 of the firing gain to shunting inhibition. This means that, on average, a shunting input equivalent to a neuron's resting conductance reduces the firing gain in

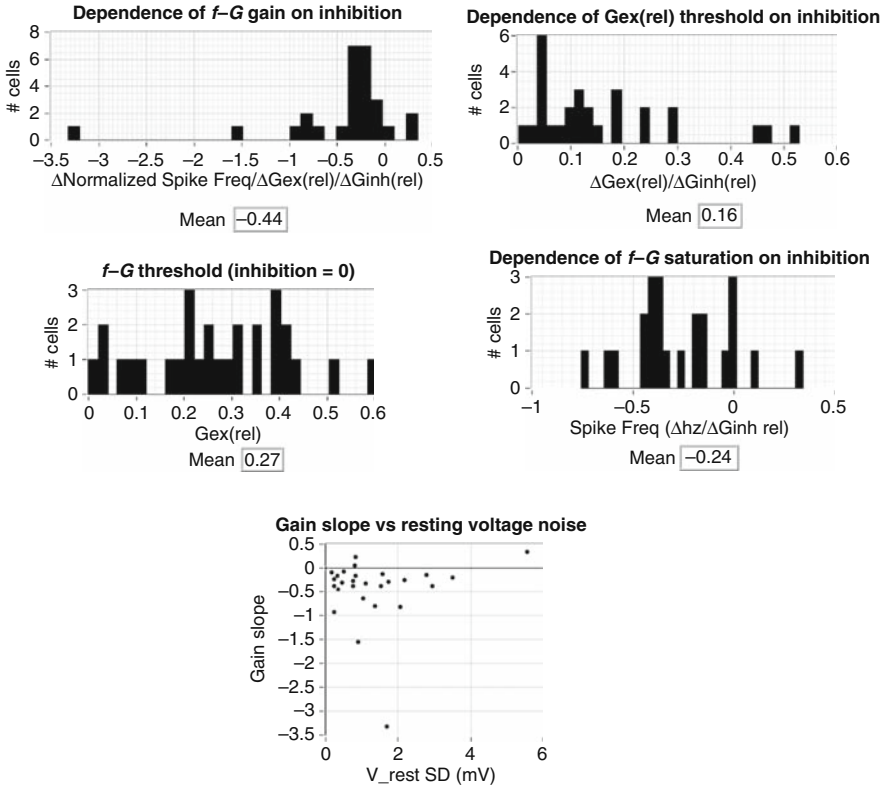

Fig. 3 Population results from 27 regular adapting neurons recorded in vivo in rat somatosensory and visual cortex ($N = 14$) and cat visual cortex ($N = 13$), quantifying the effect of artificial "shunting inhibition" on firing properties measured with *f–G* protocols. All values of excitatory and inhibitory "synaptic" dynamic-clamp conductance inputs are normalized to the resting input conductance of each neuron. Gain measures (e.g. ΔNormalized Spike Freq/ΔGex(rel)) are normalized with respect to the firing gain in the absence of artificial shunting inhibition. The "*f–G* threshold (inhibition = 0)" plot shows the distribution of minimum values of the normalized excitatory input (Gex(rel)) necessary to evoke spikes, while the "Dependence of Gex(rel) threshold on inhibition" plot shows the sensitivity of this value with simultaneous application of shunting inhibition. For the measure of "Dependence of saturation on inhibition," which shows how the measured (or in some cases extrapolated) maximum firing frequency is sensitive to shunting inhibition, a subset of 24 out of 27 neurons were analyzed which showed saturation for large values of excitation. The plot at bottom shows the lack of correlation between the gain sensitivity to inhibition ("gain slope") and the intrinsic fluctuations of the membrane potential at rest

response to synaptic excitation to 44% the gain when there is no inhibition. We also quantified the threshold excitatory synaptic input, analogous to the more classic measure of threshold current input, or rheobase. Over the population, the average minimum synaptic excitation for eliciting spikes with no inhibition was 0.27, again normalized to the resting conductance (middle left). The

sensitivity of this value with respect to the simultaneous presentation of shunting inhibition encapsulates the "linear" interaction between excitation and inhibition: Over the population the average normalized increase of the threshold excitatory input, e.g. the rightward shift of the *f–G* curve, with increasing inhibition (also normalized to the resting conductance) is 0.16 (top right). Thus, on average, for a shunting input equivalent to the resting conductance the threshold excitatory input increases by 16%.

Neuronal firing frequencies do not increase without limit for stronger inputs, and for realistic inputs the expected saturation may be relevant for coding. For those cells in our data set in for which saturation could either be measured directly or estimated (24 out of 27), we measured the effect of shunting inhibition on the saturation frequency. We found that, on average, shunting inhibition equivalent to the resting conductance of a neuron reduced the saturation firing frequency by 24% (middle right). Finally, in light of various reports describing a necessary role of noise for shunting inhibition to have a non-linear effect on firing gain, we measured the "intrinsic" voltage noise for each neuron in the resting state. From these measurements (bottom) we found no correlation between the sensitivity of firing gain to inhibition ("Gain Slope," as shown in the top left), indicating that for our experimental conditions, neither "noise" in the artificial inputs, nor "noise" intrinsic in the network are necessary to see a significant non-linear effect on firing rates between shunting inhibition and excitation.

Figure 4 illustrates the general suppression effect of artificial shunting inhibition on the visual response of a neuron in cat visual cortex. This cell showed a very tight selectivity to the orientation of a moving grating, giving a spike response only when the direction of motion was along the 90–270° axis (top right, tuning measured at 45° increments). This tuning was unchanged when a constant artificial shunting inhibitory input was added with the dynamic-clamp (middle right, Ginh(rel) = 1), whereas the number of spikes was significantly reduced by about half. Furthermore, shunting inhibition affected the coding of the response, tightening the temporal spread of the evoked spikes (compare spike times with and without the shunt, top left and middle left, respectively). Notably, the relatively strong inhibition (consistent with amplitudes evoked by visual stimuli, Borg-Graham et al., 1998; Monier et al., 2003) did not simply annihilate the response, but rather had a more nuanced effect.

5.2 *The Effects of* $\mathbf{I}_{BK}$ *on the Input–Output Function and Visual Responses*

Figure 5 illustrates the relationship between I_{BK} and spike repolarization as predicted by a biophysically detailed model (Borg-Graham, 1987, 1998), and recreated with a dynamic-clamp approximation during an in vivo recording of a rat cortical neuron with the native I_{BK} blocked with intracellular BAPTA.

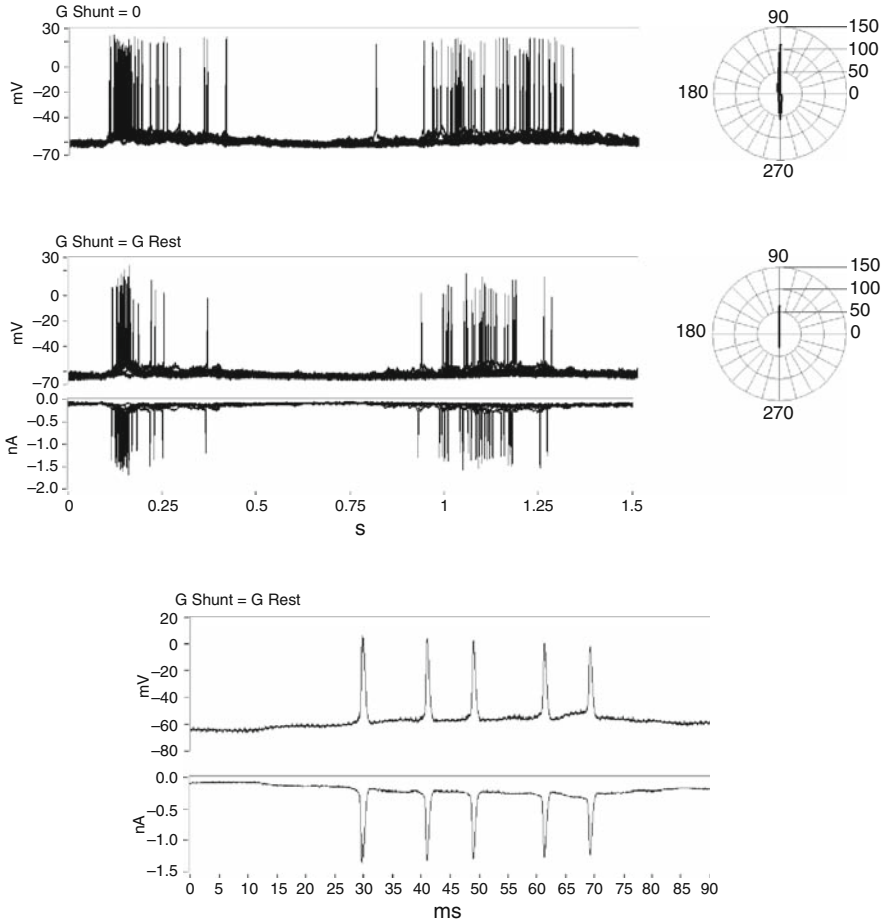

Fig. 4 The effect of artificial shunting inhibition during the visual response of a neuron in cat visual cortex in vivo. Top traces show superimposed voltage recordings of ten trials in response to a preferred stimulus (90° direction, 1 hz drifting sinusoidal grating) with the dynamic-clamp shunting inhibition turned off (G Shunt = 0) and on (G Shunt = G Rest), in the latter case showing the associated current traces supplied by the dynamic-clamp, thus the current through the "GABAA synapse." An expanded view of one response with shunting inhibition is shown in the lower traces

The simulated action potentials at the top left, in response to a short current pulse, shows the control condition with an active I_{BK} mediating the fAHP (thick trace), and the case with I_{BK} disabled (thin trace) by blocking calcium currents. The simulated membrane currents at bottom left show the principal repolarizing K^+ currents for the control condition, including I_A, I_{DR}, and I_{BK} (light gray, gray, and black traces, respectively) (adapted from Borg-Graham, 1999). The predicted repolarization trajectories with and without I_{BK} are well reproduced in the experimental recordings (right), demonstrating that the

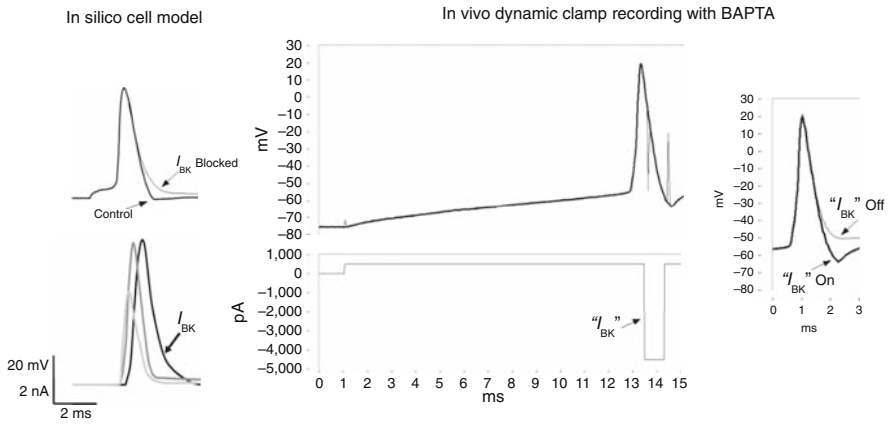

Fig. 5 Comparison of predictions of biophysically detailed model of hippocampal pyramidal cell with respect to the kinetics and voltage signature of I_{BK} (*left*), and electrophysiological dynamic-clamp recording with a simplified version of *I*BK injected during the repolarization of an action potential, of a regular adapting neuron recorded in rat somatosensory cortex in vivo (*middle and right*), with the calcium buffer BAPTA in the pipette acting to prevent full activation of the native I_{BK}. *Top middle* – Evoked action potential with I_{BK} dynamic-clamp model enabled. Thin trace is original voltage recording showing bridge artifacts from the current pulse transitions, while the thick trace has these artifacts removed by a simple algorithm that interpolates the voltage during a 200 μs interval whenever the current derivative exceeds a maximum value (here, 2nA/ms). *Bottom middle* – total clamp current supplied by recording amplifier, including a long 500 pA depolarizing step and a short "I_{BK}" pulse triggered by the repolarizing phase of the spike. Right – the same action potential from middle top (*thick trace*) superimposed with an action potential evoked by same depolarizing pulse, but with I_{BK} dynamic-clamp disabled (*thin trace*)

simple I_{BK} model captures the essential effect of this current at the level of the membrane voltage.

As mentioned earlier, the simple I_{BK} model shown here does not include a deactivation component that is seen over the first few spikes, and that we have explored in previous work (Borg-Graham, 1987, 1999; Shao et al., 1999). Therefore, this I_{BK} model provides a sort of upper bound of the effect of the native I_{BK} over a prolonged spike train. The augmentation of the overall *f–I* I/O relation by the artificial I_{BK} dynamic-clamp current is seen in Fig. 6, although the final impact on spike timing by the I_{BK} model is complex. Thus, for this cell the first interspike interval in the control case is shorter (i.e. the instantaneous frequency is higher) than that when the model I_{BK} is enabled, indicating a regime (possibly due in part to an incomplete block of the native I_{BK}) in which the extra hyperpolarizing current shows the classical effect of reducing excitability. Overall, though, for larger amplitudes of the artificial I_{BK} the interspike interval becomes shorter, being less than the control case for progressively earlier intervals (top right, for a current step of 350 pA). Again, this effect is probably larger than provided by the native I_{BK} because the model does

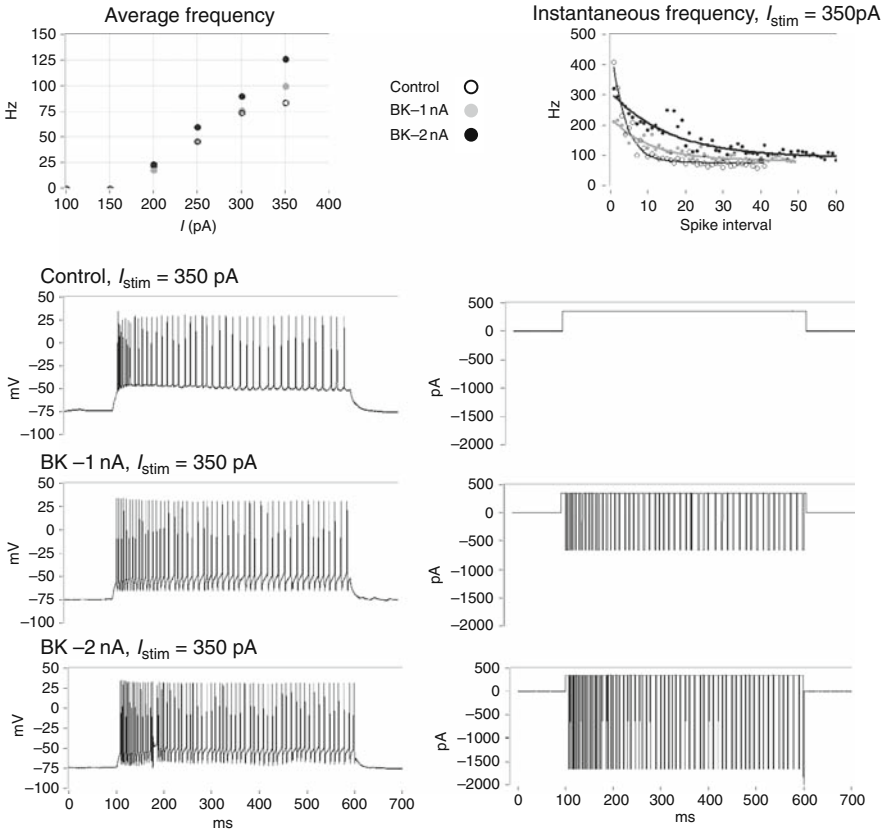

Fig. 6 I_{BK}-dependent *f–I* characteristics, measured in cat visual cortex in vivo with whole-cell patch recordings with the calcium buffer BAPTA in the pipette. The control case is with the dynamic-clamp I_{BK} disabled

not de-activate. Nevertheless, in the case of visual responses to moving gratings, as shown in Figs. 7 (rat visual cortex) and 8 (cat visual cortex), the evoked synaptic dynamics typically fluctuate to a large degree, as opposed to being steady and constant (cf. response to a current step), and therefore the lack of de-activation in the I_{BK} model is of secondary importance for these protocols. In Fig. 7, from rat visual cortex, the cell shows a relatively weak, but consistent, tuning preference for the 135–315° axis that is maintained when the overall response is increased with the dynamic-clamp I_{BK}. Figure 8, from cat visual cortex, compares the preferred response with the native I_{BK} blocked, and with the native I_{BK} replaced by the dynamic-clamp I_{BK}. The addition of I_{BK} not only increases the response, but, relevant to temporal coding, increases the "burstiness" of the evoked responses, i.e. tending to make the cell respond with a couplet or triplet of spikes, rather than just one, in response to a brief stimulus.

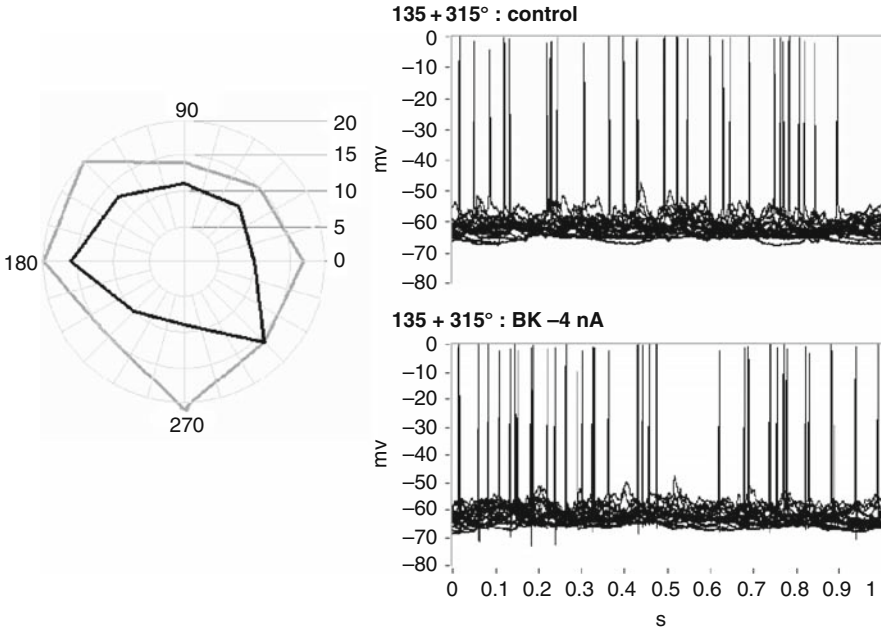

Fig. 7 I_{BK}-dependent visual response characteristics, measured in rat visual cortex in vivo with whole-cell patch recordings with the calcium buffer BAPTA in the pipette. *Left* – polar plot of total spike response over ten trials as a function of direction of drifting grating (Control, black; with dynamic-clamp I_{BK}, gray). *Right* – Preferred responses to oriented drifting grating with (*bottom*) and without (*top*) artificial I_{BK} (superimposed voltage responses of ten trials each of gratings moving toward 135 and 315°)

6 Discussion

Our results reveal that levels of shunting inhibition in the cortex, consistent with that evoked by functional stimuli, induces not only a linear shift in the spiking threshold, but also a reduction of the gain of the transfer function. This general effect holds as well for the case of visual responses. We are now working on a global quantification of this effect and on relating our findings with the previous studies. Particularly, in most previous work, the maximum shunt applied is less than or equal to the resting conductance, whereas in our protocols we test larger values of the relative shunt, which may account for some differences in the results. Moreover, we found no obvious relationship between intrinsics membrane voltage fluctuations and the sensitivity of firing gain on applied shunting inhibition, contrary to previous reports which have claimed a necessary role of "noise" in any non-linear effect of shunting inhibition. We also find that the saturation point of the transfer function is reduced with shunting inhibition. Finally, we found (Graham et al., 2007) that these effect are conserved among the various classical electrophysiological cell types in mammalian

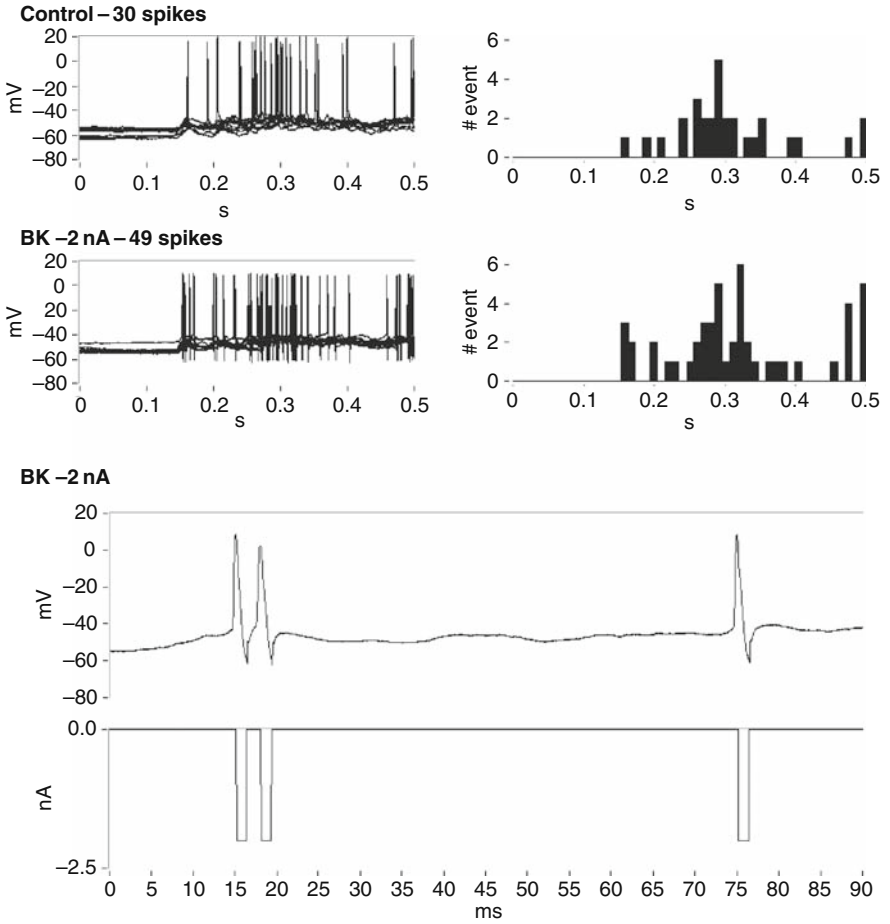

Fig. 8 I_{BK}-dependent visual response characteristics, measured in cat visual cortex in vivo with whole-cell patch recordings with the calcium buffer BAPTA in the pipette. *Top* – preferred responses to oriented moving grating without (control) and with (BK –2 nA) artificial I_{BK}. Left panels show superimposed voltage traces from ten trials, and right panels show post stimulus time histograms (PSTHs) of the evoked spike times. *Bottom* – Example voltage and dynamic-clamp current response with artificial I_{BK}. Compare with the similar hyperpolarizing spike currents supplied by artificial shunting inhibition in Fig. 4 (*bottom*)

cortex, thus regular adapting, fast spiking and bursting neurons (data not shown), which emphasizes the general importance of shunting inhibition control on neuronal information processing.

Our results on I_{BK} confirm previous hypotheses that this current, although hyperpolarizing, actually serves to accelerate the neuronal response. We verified this prediction at the biophysical level with our in vivo protocols by applying a minimal I_{BK} model with the native I_{BK} attenuated by the addition

of the calcium buffer BAPTA in the recording pipette. The simple I_{BK} model accelerated the response not only evoked by injected current steps, but also during "natural" visual responses.

It is interesting to contrast the complementary effects of shunting inhibition and I_{BK}, especially if we consider that, on one hand, in general both membrane currents act in opposition to depolarizing inputs, since both have reversal potentials near or below the resting potential. On the other hand, in particular as implemented in these experiments, the two mechanisms have completely complementary kinetics: The shunting inhibition model that we tested is essentially a tonic conductance input with no intrinsic kinetics, whereas the model I_{BK} kinetics are extremely precise, adjusted to exclusively sculpt the repolarizing phase of individual action potentials. The contrast can be appreciated by the example plots of the shunting inhibition current and I_{BK} at the bottom of Figs. 4 and 8, respectively. To a first approximation, the dynamic-clamp protocol supplies similar negative currents in the two cases, but indeed the fact that the kinetics are so different causes a qualitatively different effect on spiking. Thus, the divergent effects on spiking output underline the point that neuronal dynamics arise from a complex, and non-obvious, interaction of non-linear mechanisms in the single cell.

For shunting inhibition and I_{BK} our results suggest not only a general down- or upregulation, respectively, of the evoked response by these mechanisms, but also more subtle effects on the precise pattern of evoked spikes. The results have implications on how these extrinsic and intrinsic membrane mechanisms may impact the neural code, whether or not a rate-based code or timing-based code, or something in between, turns out to the be relevant language of the brain. In the final analysis it is essential to consider the fine details of various mechanisms such as these in order to establish the functional roles of the elements comprising the neuron's biophysical mosaic (Graham and Kado, 2002). The application of the dynamic-clamp method in vivo to address quantitative properties of biophysical mechanisms of neurons which are as close as possible to their natural state, and in the context of realistic functional responses, will be an essential tool toward this understanding.

Acknowledgments This work was supported by an HFSP grant (RGP0049/2002) and an Agence Nationale de Recherche grant (FUNVISYNIN) to Dr. Lyle J. Graham. We also gratefully acknowledge Thomas Gener for his help in developing the protocols and participating in early experiments. We also acknowledge the important contribution of the authors of the VisionEgg and the G-Clamp software packages.

References

Anderson J, Carandini M, Ferster D (2000) Orientation tuning of input conductance, excitation and inhibition in cat primary visual cortex. J Neurophysiol 84:909–26.

Anderson J, Lampl I, Gillespie D, Ferster D (2001) Membrane potential and conductance changes underlying length tuning of cells in cat primary visual cortex. J Neurosci 21:2104–12.

Bernander O, Douglas RJ, Martin KAC, Koch C (1991) Synaptic background activity influences spatiotemporal integration in single pyramidal cells. Proc Natl Acad Sci USA 88:11569–73.

Borg-Graham LJ (1987) Modelling the somatic electrical behaviour of hippocampal pyramidal neurons. MSEE Thesis, Massachusetts Institute of Technology.

Borg-Graham L, Monier C, Frégnac Y (1998) Visual input evokes transient and strong shunting inhibition in visual cortical neurons. Nature 389:369–73.

Borg-Graham LJ (1999) Interpretations of data and mechanisms for hippocampal pyramidal cell models. In Cerebral cortex, eds. Ulinski PS, Jones EG, & Peters A, pp. 19–138. Kluwer Academic/Plenum Publishers, New York.

Brizzi L, Meunier C, Zytnicki D, Donnet M, Hansel D, LaMotte D'Incamps B, Van Vreeswijk C (2004) How shunting inhibition affects the discharge of lumbar motoneurones. A dynamic clamp study in anaesthetised cats. J Physiol 558(Pt 2):671–83.

Capaday C, Van Vreeswijk C (2006) Direct control of firing rate gain by dendritic shunting inhibition. J Integr Neurosci 5:199–222.

Chance FS, Abbott LF, Reyes AD (2002) Gain modulation from background synaptic input. Neuron v35, 773–82.

Destexhe A, Paré D (1999) Impact of network activity on the integrative properties of neocortical pyramidal neurons in vivo. J Neurophysiol 81:1531–47.

Fellous J-M, Rudolph M, Destexhe A, Sejnowski TJ (2003) Synaptic background noise controls the input/output characteristics of single cells in an in vitro model of in vivo activity. Neuroscience 122:811–29.

Graham L, Kado R (2002) The neuron's biophysical mosaic and its computational relevance. In the Handbook for Brain Theory and Neural Networks, ed. Arbib M, 2nd edition, pp. 170–175. MIT Press.

Graham LJ (2006) Not what you'd expect: Paradoxical roles of Na+ and K+ currents on excitability. Paper presented at the Modelling the Brain's Labyrinth Meeting, Hieraklion, Greece.

Graham LJ (2007) Not what you'd expect: Paradoxical roles of Na+ and K+ currents on excitability. Paper presented at the Quantitative Neuron Modeling Meeting, EPFL, Lausanne, Switzerland.

Graham LJ, Schramm A, Gener T (2007) The modulation of firing gain and threshold by shunting inhibition in cortical neurons in vivo, Society for Neuroscience Annual Meeting Abstracts, San Diego, USA.

Gu N, Vervaeke K, Storm JF (2007) BK potassium channels facilitate high-frequency firing and cause early spike frequency adaptation in rat CA1 hippocampal pyramidal cells. J Physiol 580(3):859–82.

Haider B, Duque A, Hasenstaub A, McCormick D (2006) Neocortical network activity in vivo is generated through a dynamic balance of excitation and inhibition. J Neurosci 26:4535–45.

Haider H, Duque A, Hasenstaub AR, Yu Y, McCormick DA (2007) Enhancement of visual responsiveness by spontaneous local network activity in vivo. J Neurophysiol 4186–202.

Higley M, Contreras D (2006) Balanced excitation and inhibition determine spike timing during frequency adaptation. J Neurosci 26:448–57.

Hirsch JA, Alonso JM, Reid RC, Martinez LM (1998) Synaptic integration in striate cortical simple cells. J Neurosci 18:9517–28.

Holt G.R, Koch C (1997) Shunting inhibition does not have a divisive effect on firing rates. Neural Comput 9:1001–13.

Ingham NJ, McAlpine D (2005) GABAergic inhibition controls neural gain in inferior colliculus neurons sensitive to interaural time differences. J Neurosci 25(26):6187–98.

Kullmann PHM, Wheeler DW, Beacom J, Horn JP (2004) Implementation of a fast 16-bit dynamic clamp using LabVIEW-RT. J Neurophysiol 91:542–54.

Kreiner L, Jaeger D (2003) Synaptic shunting by a baseline of synaptic conductances modulates responses to inhibitory input volleys in cerebellar Purkinje cells. Cerebellum 3:112–25.

Manuel M, Meunier C, Donnet M, Zytnicki D (2005) How much afterhyperpolarization conductance is recruited by an action potential? A dynamic-clamp study in cat lumbar motoneurons. J Neurosci 25(39):8917–23.

Marino J, Schummers J, Lyon D, Schwabe L, Beck O, Wiesing P, Obermayer K, Sur M (2005) Invariant computations in local cortical networks with balanced excitation and inhibition. Nat Neurosci 8:194–201.

Marrion NV, Tavalin SJ (1998) Selective activation of Ca2 + -activated K + channels by co-localized Ca2 + channels in hippocampal neurons. Nature 395:900–5.

McCormick DA, Connors BW, Lighthall JW, Prince DA (1985) Comparative electrophysiology of pyramidal and sparsely spiny neurons of the neocortex. J Neurophysiol 54:782–806.

Mitchell SJ, Silver RA (2003) Shunting inhibition modulates neuronal gain during synaptic excitation. Neuron 38:433–45.

Monier C, Chavane F, Baudot P, Graham L, Frégnac Y (2003) Orientation and direction selectivity of excitatory and inhibitory inputs in visual cortical neurons: A diversity of combinations produces spike tuning. Neuron v37:663–80.

Prescott SA, De Koninck YD (2003) Gain control of firing rate by shunting inhibition: Roles of synaptic noise and dendritic saturation. Proc Natl Acad Sci USA 100(4):2076–81.

Priebe N, Ferster D (2005) Direction selectivity of excitation and inhibition in simple cells of the cat primary visual cortex. Neuron 45:133–45.

Priebe N, Ferster D. (2006) Mechanisms underlying cross-orientation suppression in cat visual cortex. Nat Neurosci 9:552–61.

Rapp M, Yarom Y, Segev I (1992) The impact of parallel fiber background activity on the cable properties of cerebellar Purkinje cells. Neural Comput 4:518–33.

Rudolph M, Destexhe A (2003) A fast-conducting, stochastic integrative mode for neocortical neurons in vivo. J Neurosci 23:2466–76.

Schramm A, Graham LJ (2007) Touch 'n Zap: A new technique for blind whole-cell patch recordings, 8e Colloque de la Société des Neurosciences, Montpellier, France.

Semyanov A, Walker MC, Kullmann DM, Silver RA (2004) Tonically active GABA A receptors: modulating gain and maintaining the tone. Trends Neurosci 27(5): 262–9.

Shao LR, Halvorsrud R, Borg-Graham L, Storm JF (1999) The role of BK-type Ca2 + -dependent K + channels in spike broadening during repetitive firing in rat hippocampal pyramidal cells. J Physiol v521.1:135–46.

Stell BM, Brickley SG, Tang CY, Farrant M, Mody I (2003) Neuroactive steroids reduce neuronal excitability by selectively enhancing tonic inhibition mediated by {delta} subunit-containing GABAA receptors. PNAS 100(24):1443.

Storm J F (1990). Potassium currents in hippocampal pyramidal cells. Prog Brain Res 83:161–87.

Storm J, Borg-Graham L, Adams P (1987) A passive component of the afterdepolarization (ADP) in rat hippocampal cells. Biophys J 51:65a.

Straw AD, Warrant EJ, O'Carroll DC (2006) A 'bright zone' in male hoverfly (*Eristalis tenax*) eyes and associated faster motion detection and increased contrast sensitivity. J Exp Biol 209(21):4339–54.

Tan AY, Zhang LI, Merzenich MM, Schreiner CE. (2004) Tone-evoked excitatory and inhibitory synaptic conductances of primary auditory cortex neurons. J Neurophysiol 92:630–43.

Ulrich D (2003) Differential arithmetic of shunting inhibition for voltage and spike rate in neocortical pyramidal cells. Eur J Neurosci 18:2159–65.

Velumian AA, Carlen PL (1999) Differential control of three after-hyperpolarizations in rat hippocampal neurones by intracellular calcium buffering. J Physiol 517:201–16.

Vergara C, Latorre R, Marrion NV, Adelman JP (1998) Calcium-activated potassium channels. Curr Opin Neurobiol 8:321–9.

Wehr M, Zador AM (2003) Balanced inhibition underlies tuning and sharpens spike timing in auditory cortex. Nature 426:442–6.
Wehr MS, Zador A (2005) Synaptic mechanisms of forward suppression in rat auditory cortex. Neuron 47:325–7.
Wilent W, Contreras D (2004) Synaptic responses to whisker deflections in rat barrel cortex as a function of cortical layer and stimulus intensity. J Neurosci 24:3985–98.
Wilent W, Contreras D (2005) Dynamics of excitation and inhibition underlying stimulus selectivity in rat somatosensory cortex. Nat Neurosci 8:1364–70.
Zhang LI, Tan AY, Schreiner CE, Merzenich MM (2003) Topography and synaptic shaping of direction selectivity in primary auditory cortex. Nature 424:201–5.